Original Research

Induced Magnetic Force in Human Heads Exposed to 4 T MRI

Ruiliang Wang, PhD,[1]* Gene-Jack Wang, MD,[1] Rita Z. Goldstein, PhD,[1] Elisabeth C. Caparelli, PhD,[1,2] Nora D. Volkow, MD,[3,4] Joanna S. Fowler, PhD,[1] and Dardo Tomasi, PhD[1,3]

Purpose: To map the distribution of the magnetic force induced in the human head during magnetic resonance imaging (MRI) at 4 T for a large group of healthy volunteers.

Materials and Methods: The magnetic field distribution in the head of 100 men and 18 women was mapped using phase mapping techniques. Statistical parametric mapping methods using a family-wise error (FWE) corrected threshold $P < 0.05$ and region-of-interest analyses were used to assess the significance of the results.

Results: Eyeballs, orbitofrontal and temporal cortices, subcallosal gyrus, anterior cingulate, midbrain, and brainstem (pons) are the brain regions most susceptible to magnetic force. The strength of the magnetic force density in the head was lower than 11.5 ± 5.3 N/m^3 (right eyeball). The strength of the magnetic force density induced in occipital cortex varied linearly with the x-rotation (pitch) angle.

Conclusion: We found that the induced magnetic force is highly significant in the eyeballs, orbitofrontal and temporal cortices, subcallosal gyrus, anterior cingulate as well as midbrain and brainstem (pons), regardless of subjects' age or gender. The maximum induced magnetic force was 6×10^5 times weaker than the gravitational force; thus, biological effects of the magnetic force during imaging are not expected to be significant.

Key Words: magnetic resonance imaging; magnetic gradient field; induced magnetic force; MRI safety; phase mapping; ROI analysis; susceptibility-weighted MR pulse sequence

J. Magn. Reson. Imaging 2010;31:815–820.

MAGNETIC RESONANCE IMAGING (MRI) has become one of the safest medical techniques (1). However, with the steady progress of MRI technology, from lower to higher magnetic field strengths, potential adverse effects of the increasing magnetic force on living tissues are calling for more attention (2). Because of safety concerns, there is a myriad of studies evaluating the magnetic force on medical devices exposed to MRI (reviewed in Refs. 2–4). However, less attention has been given to effects of the magnetic force on living tissues during MRI scanning procedures. While in an earlier study on positron emission tomography it was reported that no effects of a 4 T static magnetic field on brain glucose metabolism, which is a marker of brain function (5), a few studies have associated dizziness (3), vertigo (1), magnetophosphenes (4), and metallic taste (6) to exposure to high magnetic fields in humans, and the quantification of the spatial distribution of the magnetic force in humans and animals during MRI scans is still lacking. Our recent quantitative measurements of the magnetic force distribution in the head of one human subject during 4 T MRI (7) reveled that the magnetic force induced in tissues of the human head during MRI procedures was lower than 0.1% of the gravitational force applied on the same tissues, suggesting a minimal impact of the MRI static magnetic field on biological tissues (7). However, the induced magnetic force in tissues can vary due to brain shape differences across subjects and/or the orientation of the head with respect to the static magnetic field. Therefore, the purpose of the current study was to evaluate the magnetic force applied on biological tissues in the human head during standard MRI procedures in a large group of subjects (>100 healthy subjects). Based on our previous single-subject measurements (7) and previous numerical simulations by others (8), we hypothesized that the induced magnetic force during MRI scans would be highly significant across subjects in the eyeballs and in the vicinities of the sinus cavity (orbitofrontal

[1]Medical Department, Brookhaven National Laboratory, Upton, New York, USA.
[2]SCAN Center, Stony Brook University, Stony Brook, New York, USA.
[3]National Institute on Alcoholism and Alcohol Abuse, Bethesda, Maryland, USA.
[4]National Institute on Drug Abuse, Bethesda, Maryland, USA.

*Address reprint requests to: R.W., Brookhaven National Laboratory, Bldg. 555A, Upton, NY 11973. E-mail: rlwang@bnl.gov

Received October 7, 2009; Accepted January 8, 2010.
DOI 10.1002/jmri.22125
Published online in Wiley InterScience (www.interscience.wiley.com).

cortex) and the temporal bones (temporal cortex). For this purpose we mapped the induced magnetic field and the induced magnetic force in the head of 118 healthy human subjects using 4 T MRI and phase-mapping techniques using a susceptibility-weighted MR pulse sequence (7,9,10).

MATERIALS AND METHODS

Subjects

A total of 118 healthy volunteers (100 males, 18 females; age = 35.5 ± 17.5), who provided written consent approved by the local Institutional Review Board, participated in this study. Subjects were included if they were older than 18 years and younger than 60 years and excluded for 1) history of head trauma or loss of consciousness (> 30 min); 2) abnormal vital signs at time of screening or history of major medical conditions; 3) pregnancy as confirmed with a urine test in all females; and 4) contraindications to MRI.

MRI Acquisition

Imaging was carried out in a 4 T Varian/Siemens MRI scanner. The homogeneity of the static magnetic field was maximized for a spherical and uniform water phantom (ID = 15 cm) using a 1D-FID NMR experiment by means of first- and second-order active shimming channels; the magnetic field homogeneity was better than 0.05 ppm in the volume of the phantom. These shimming parameters were fixed across subjects to minimize shimming-related magnetic field gradient differences across subjects. A fast low angle shot (FLASH) pulse sequence (11) with 31 sagittal slices; 4 mm thickness; 1 mm gap; in-plane resolution = 1.56 mm; acquisition matrix = 128 × 128; TR = 0.3 seconds; TE_1 = 4 msec, TE_2 = 5 msec; total scan time 4 minutes; phase-encoding gradient step = 0.18 mT/m; slice selection gradient = 5.25 mT/m; readout gradient = 9.81 mT/m; acquisition bandwidth = 83.59 kHz was used to measure the magnetic force distribution in the subjects' heads. Anatomical images were acquired using a T1-weighted 3D-MDEFT sequence (12) (TE/TR = 7/15 msec, 0.94 × 0.94 × 1 mm spatial resolution, axial orientation, 256 readout and 192 × 96 phase-encoding steps, 16 min scan time), and a modified T2-weighted Hyperecho sequence (13) (TE/TR = 42/10,000 msec, echo train length = 16, 256 × 256 matrix size, 30 coronal slices, 0.86 × 0.86 mm in-plane resolution, 5 mm thickness, no gap, 2.5-minute scan time), which were carefully reviewed to rule out major morphological abnormalities in the brain.

Calculation of Magnetic Field Gradients and Forces

The longitudinal component of the magnetic field distribution, $B_z(\mathbf{r}) = \gamma^{-1}\,\phi(\mathbf{r}, TE_2 - TE_1) * (TE_2 - TE_1)^{-1}$, was calculated from differential phase maps, $\phi(\mathbf{r}, TE_2 - TE_1)$, resulting from the complex ratio between FLASH datasets with TE = 5 msec and TE = 4 msec. This allowed us to minimize phase wrapping artifacts. The magnetic field gradient maps were calculated from magnetic field differences between adjacent voxels:

$$\mathbf{g}(\mathbf{r}) = \nabla(B_z(\mathbf{r})) = \left(\frac{\partial B_z(\mathbf{r})}{\partial x}, \frac{\partial B_z(r)}{\partial y}, \frac{\partial B_z(r)}{\partial z}\right) \quad [1]$$

The magnetic force acting on biological tissues, which is proportional to their isotropic magnetic susceptibility (14), $\chi \ll 1$, was calculated according to:

$$F_z = \frac{\chi V}{\mu_0} B_0 \frac{\partial B_z}{\partial z}, \quad [2]$$

where V is the voxel volume, B_0 is the static magnetic field strength, and μ_0 stands for the vacuum permeability. A customized algorithm, computing Eqs. [1] and [2] voxel-by-voxel, was developed in IDL (ITT Visual Information Solutions, Boulder, CO) to calculate $\mathbf{g}$ and F_z.

Statistical Analyses

The Statistical Parametric Mapping (SPM2; Wellcome Department of Cognitive Neurology, London, UK) package was used for imaging postprocessing. The magnitude image corresponding to TE = 4 msec was spatially normalized to the standard frame (Talairach) with a 12-parameters affine transformation (15) using the standard T2* template provided with the SPM2 package, and these parameters were used for the spatial normalization of the calculated maps (g_x, g_y, g_z, and F_z) using a voxel size of 3 × 3 × 3 mm. An 8-mm full-width-half-maximum (FWHM) Gaussian kernel was used to smooth the maps of the induced magnetic field gradients and forces, which were subsequently entered into a general linear model in SPM2 for group analyses. Independent analyses were carried out for each gradient component (g_i) and F_z. The statistical significance of the induced field gradients and forces was evaluated voxel-by-voxel across subjects using one-sample t-test (random-effect) models and a family-wise error (FWE) threshold $P_{corr} < 0.05$, corrected for multiple comparisons with the continuous random field calculation implemented in SPM2.

Region of Interest (ROI) Analyses

The magnetic force distribution was further evaluated with ROI analyses to identify potential outliers that might influence linear regressions and to report average values in a volume comparable to the image smoothness (e.g., resolution elements, or "resels" (16) rather than single-voxel peak values. The volume of the resels was estimated using the random field calculation in SPM2 as a near isotropic volume with FWHM = 6 mm. Thus, the magnetic force distribution was evaluated across subjects in 19 ROIs using 9-mm isotropic cubic masks containing 27 imaging voxels (0.729 mL) and centered at the Talairach coordinates listed in Table 1. The strength and standard deviation of the magnetic field gradients and forces induced by tissue susceptibility within these fixed masks was calculated across subjects using a custom program

Table 1
Location of ROIs in the Talairach Frame of Reference and the Induced Magnetic Gradients (*x,y,z*) and Forces in Specific ROIs

ROI	Brain		*x*	*y*	*z*	ΔB_0		ΔGx		ΔGy		ΔGz		MF	
	Region	BA	mm	mm	mm	ppm	SD	mT/m	SD	mT/m	SD	mT/m	SD	pN	SD
1	ITG	37	−55	−41	−19	−0.45	2.63	0.03	0.069	−0.050	0.092	−0.09	0.074	−32.6	26.1
2	ITG	37	55	−41	−19	0.61	2.81	−0.13	0.102	−0.030	0.163	−0.11	0.13	−39.7	45.6
3	ITG		−54	−10	−19	−0.68	2.70	−0.02	0.048	0.046	0.076	0.09	0.059	30.8	20.5
4	ITG		54	−10	−19	0.2	3.05	−0.04	0.060	0.092	0.096	0.09	0.078	33.1	27.3
5	CT		−21	−68	−32	−0.75	2.87	−0.02	0.033	0.072	0.031	0.05	0.025	18.4	8.7
6	CT		21	−68	−32	−0.45	3.02	−0.04	0.035	0.077	0.033	0.05	0.026	16.3	9.2
7	LEB		−33	48	−37	−0.26	2.39	−0.10	0.130	0.089	0.195	0.49	0.225	172.9	78.8
8	REB		33	48	−37	0.09	2.67	0.07	0.150	0.050	0.222	0.34	0.313	120.6	109.8
9	MFG		−1	46	−16	0.37	2.64	−0.05	0.056	−0.020	0.160	0.12	0.085	43.1	29.7
10	SG	25	−1	5	−16	0.27	2.79	−0.06	0.062	0.005	0.138	−0.26	0.153	−89.5	53.5
11	SG		−46	−12	−8	−0.5	2.68	−0.01	0.036	0.057	0.028	0.04	0.027	−32.6	26.1
12	SG		46	−12	−8	0.35	2.97	−0.06	0.039	0.076	0.043	0.04	0.032	12.2	9.6
13	AC	25	−1	5	−8	0.16	2.79	−0.05	0.048	0.010	0.086	−0.13	0.084	13.2	11.3
14	MFG	10	−2	48	−8	0.37	2.69	−0.05	0.045	−0.010	0.079	0.06	0.067	−46.5	29.5
15	IFG	47	−51	20	0	−0.46	2.67	−0.04	0.045	0.069	0.053	0.04	0.028	20.0	23.6
16	IFG	47	51	20	0	0.55	2.88	−0.04	0.049	0.073	0.054	0.03	0.04	13.5	10
17	SG		−23	−81	0	−0.31	2.73	−0.02	0.032	0.045	0.030	0.02	0.021	11.9	13.5
18	LG		23	−81	0	0.02	2.87	−0.04	0.031	0.052	0.030	0.02	0.021	8.2	7.3
19	Pons		1	−30	−36	−0.92	3.01	−0.03	0.033	0.088	0.075	0.08	0.083	5.6	7.4

pN, pico Newton or 10^{-12} Newton; ITG, inferior temporal gyrus; CT, cerebellar tonsil; MFG, medial frontal gyrus; SG, subcallosal gyrus; AC, anterior cingulate; MFG, medial frontal gyrus; IFG, inferior frontal gyrus; LG, lingual gyrus; LEB, L. eyeball; REB, R. eyeball; SG, subgyral.

written in IDL and used in subsequent correlation analyses with age and orientation of the head in the MRI scanner. A threshold $P_{corr} < 0.05$, corrected for multiple comparisons (Bonferroni), was considered statistically significant in ROI analyses.

Head Orientation

The magnitude image corresponding to TE = 4 msec was registered to a standard template using a rigid body transformation in SPM2. The calculated *x*-, *y*-, and *z*-rotation angles and the *x*-, *y*-, and *z*-translations for each subject were used in subsequent correlation analyses to evaluate head orientation-related effects on the distribution of the magnetic force in the head.

RESULTS

Induced Magnetic Field Gradients

Fig. 1A illustrates the ROIs discussed in the text and listed in Table 1. The highly heterogeneous pattern of induced magnetic field gradients reflected susceptibility differences at air–tissue interfaces near the sinus cavity and the temporal bone (Fig. 1, Table 1). Across subjects, g_z and g_y had a symmetric distribution with respect to the middle sagittal plane; they were negative in the inferior temporal (ITG, BA 37), subcallosal (SG, BA 25), anterior cingulate (AC, BA 25), and medial frontal (MFG, BA 25, ventral AC) gyri (> -1.15 mT/m) and positive in the eyeballs, the inferior frontal gyrus (IFG, BA 20, ventral temporal), the cerebellar tonsil, and MFG (BAs 10 and 11) (< 1.3 mT/m) (Fig. 1B, Table 1). On the other hand, g_x exhibited an antisymmetric pattern (Fig. 1C, Table 1), being positive in the left ITG (< 0.3 mT/m) but negative in the right ITG (> -0.53 mT/m).

Induced Magnetic Force

The distribution of F_z was similar to that of g_z as a consequence of Eq. [2] (Fig. 1E). The magnetic force was minimal in deep brain regions but maximal in the eyeballs (< 250 pN) and at the air/tissue interfaces near the sinus cavity and temporal bones (Fig. 1E). The SG (across individuals, $F_z < 150$ pN), MFG (< 80 pN), and AC (< 50 pN) were the brain regions exhibiting the highest magnetic force levels during MRI. The induced magnetic force in the human head in these regions was highly significant (T-score > 30; $P_{corr} < 0.0001$; Fig. 1F). The average F_z values were not statistically different for men and women (Fig. 2) and there were no statistically significant correlations between age and F_z either.

The lingual gyrus (BA = 23) was the only brain region that showed a statistically significant linear correlation between F_z and the head-orientation parameters. Specifically, the induced magnetic force in the lingual gyrus increased with the *x*-rotation (pitch) angle ($R = 0.4$; $P_{corr} < 0.0001$, Fig. 3, regression slope $= 0.023 \pm 0.005$ $Nm^{-3}deg^{-1}$).

There were no correlations between other head orientation parameters (*x*-, *y*-, and *z*-translations; *y*- and *z*-rotations) and F_z in the lingual gyrus, or between any of the six head orientation parameters and F_z in any of the remaining ROIs in the brain.

DISCUSSION

Here we summarize our brain mapping results of the induced magnetic field and forces acting on biological tissues in the head of 118 healthy human subjects exposed to the homogeneous static magnetic field of a 4 T MRI scanner. As far as our knowledge reaches, this study is the first to assess the distribution of

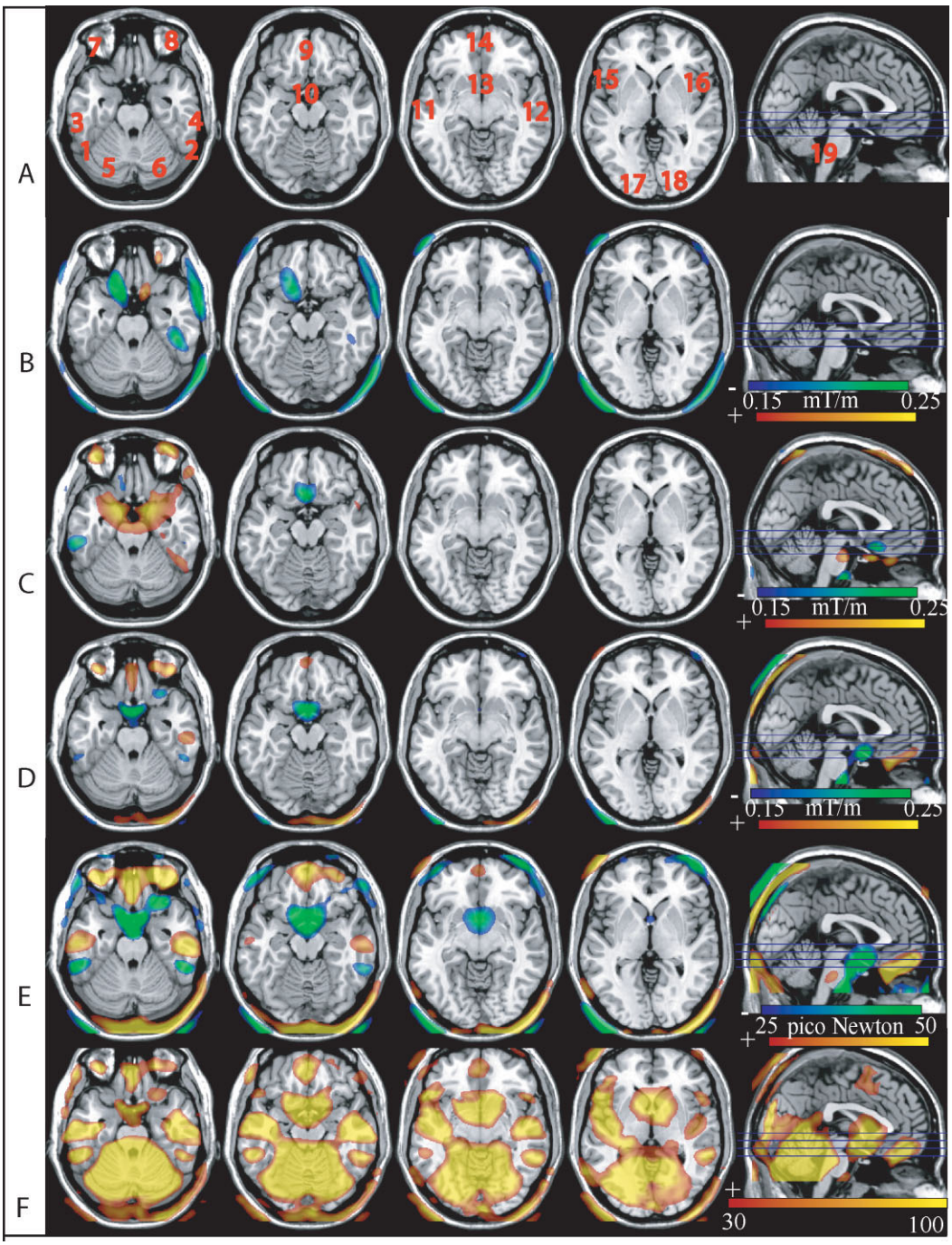

Figure 1. High-resolution axial MRI slices and labels indicating the locations of ROIs as displayed in Table 1 (**A**; ROIs marked on SPM2 template ch2.nii). Axial views of the x, y, and z components of the induced magnetic field gradient (**B–D**; all in mT/m, calculated using Eq. [1]), the average magnetic force (**E**; in pN from Eq. [2]), and the statistical maps of F_z scores showing the statistical significance of gradient and magnetic force distributions (**F**; no unit) across 118 healthy subjects superimposed on the structural MRI.

magnetic field gradients and forces in a large cohort of human subjects, thus providing an important database toward better assessment of MR safety and potential physiological effects of static magnetic fields in humans. Our main finding is that the magnetic force induced by magnetic susceptibility differences at air/tissue interfaces in the head is highly significant across all subjects. As demonstrated by our correlation analysis, only in certain regions such as the right lingual gyrus was the distribution of magnetic force significantly affected by the orientation of the head, relative to that of the magnetic field.

The magnetic force applied on weakly magnetic/diamagnetic biological tissues immersed in a perfectly homogenous external magnetic field is proportional to the local field strength, the magnetic susceptibility of the tissues, χ, and the inhomogeneity of the local magnetic field (ie, the static magnetic field gradient,

g), which reflects the geometry of tissue magnetic susceptibility differences, $\Delta\chi$ (7,14,17).

The average magnetic force in the human head was maximal at the eyeballs and the orbitofrontal and temporal cortices (Fig. 1, Table 1), consistent with previous calculations of the induced static magnetic field in the human head (8) and previous findings in a single individual (7). These regions include the hypothalamus, which controls body temperature as well as other autonomic functions, and the vestibular system that contributes to our balance and our sense of spatial orientation. Thus, our results are also consistent with the higher occurrence of tonic vestibular asymmetry, hyperreactive caloric responses, and spontaneous nystagmus documented after 30 minutes exposure to 9.4 T static field in a small group of MRI workers (18). Vestibular dizziness has been shown to deactivate the middle/medial superior temporal area (MT/MST) (19), and the same area was found to be associated with taste perceptions using different taste stimuli (20). Thus, our findings on induced magnetic force across all subjects in the ITG (Fig. 1E,F) suggest that feelings of dizziness, vertigo, and "metallic taste" after exposure to high-field MRI could be associated with neurostimulation induced by magnetic force in the ITG and the other mentioned regions. However, at current magnetic fields no such symptoms were observed/reported in this cohort of subjects.

Lingual gyrus was the only brain region that showed a statistically significant linear correlation between F_z and head orientation parameters (x-rotation, or pitch) (Fig. 3). This finding could be associated with the sensation of vertigo in the MRI scanner. The sensation of vertigo is frequently experienced when subjects move in and out of the MRI scanner, and could result from electrical currents induced in moving brain tissues exposed to magnetic fields (14). However, when the head motion is perpendicular to the orientation of the magnetic field it can induce sensations of vertigo in humans and this has been postulated to arise from magnetohydrodynamic forces giving rise to similar effects as those seen in travel sickness (21). Since the lingual gyrus was shown to activate in previous functional MRI studies on vertigo (1,22), our findings on orientation-dependent induction of magnetic forces in the lingual gyrus suggest that the magnetic force acting in these brain regions could originate sensations of vertigo in MRI (3,4,22), although these sensations would be much weaker comparing to that caused by motion in the static magnetic field (e.g., 1,3,4,6,22,23). Finally. This study does not support significant gender or aging differences in the magnetic force distribution in the human heads.

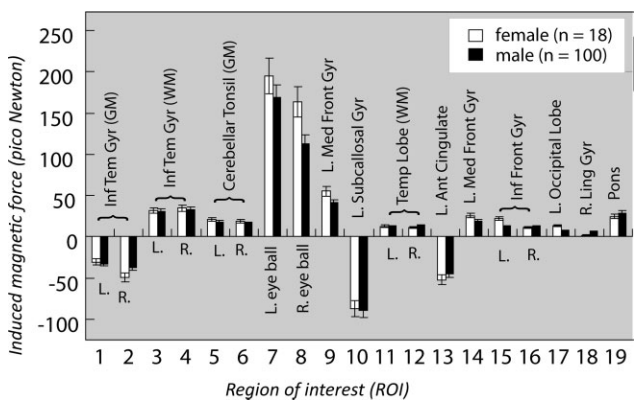

Figure 2. Induced magnetic force in ROIs (please refer to Table 1) for 100 men and 18 women. (For anatomic regions of ROIs please refer to Table 1; induced magnetic force is in pN; all tissues are assumed to have the magnetic susceptibility of pure water).

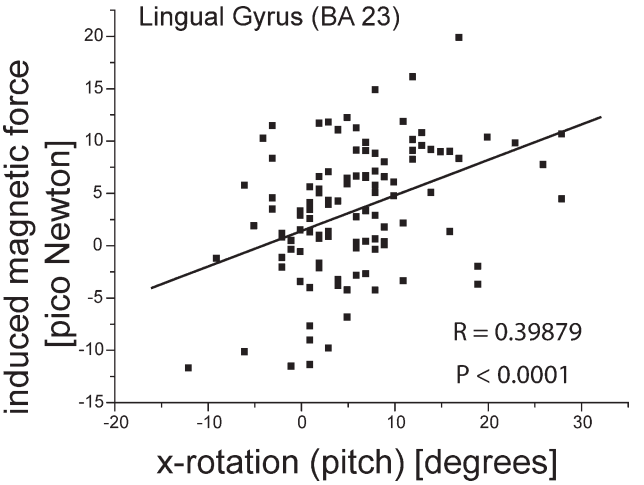

Figure 3. Linear regression between the induced magnetic force (pN) in the imaging voxel as a function of the x-rotation (pitch) angle of the head. Brain region: lingual gyrus, BA 23 (Table 1). Voxel size: 1.7 × 1.7 × 5.0 mm.

The amplitude of the imaging gradients and the acquisition bandwidth limited the accuracy of the measurements (estimated systematic error ≈ 3%). Furthermore, the measurements reflected average values within the imaging voxels. Thus, future studies using higher spatial resolution might allow detection of higher peak values for the magnetic force in the human head. This study evaluated the induced force during real MRI scan only; it does not measure the magnetic force while subjects entering or exiting the magnet, which at 4 T could be 300 times higher than that reported in this study depending on the motion speed of the body.

In conclusion, we assessed the magnetic force distribution in the head of 118 healthy humans exposed to 4 T magnetic field MRI using statistical parametric mapping techniques. We found that the induced magnetic force is highly significant in the eyeballs, orbitofrontal and temporal cortices, subcallosal gyrus, anterior cingulate as well as midbrain and brainstem (pons), regardless of subjects age or gender. The induced magnetic force was 6×10^5 times weaker than the Earth's gravitational force. While biological damage caused by the induced magnetic force in the brain during MRI scanning seems unlikely, at least under current strength of MRI technology, the

potential effects of the magnetic force on brain function merits further evaluation since it could affect activation/deactivation signal observed with fMRI studies.

ACKNOWLEDGMENT

We thank two anonymous reviewers for many constructive comments and useful suggestions on the article.

REFERENCES

1. Glover P, Cavin I, Qian W, Bowtell R, Gowland P. Magnetic-field-induced vertigo: a theoretical and experimental investigation. Bioelectromagnetics 2007;28:349–361.
2. Shellock F. Reference manual for magnetic resonance safety, implants, and devices, 2008 ed. Los Angeles: Biomedical Research Publishing Group; 2008.
3. Chakeres D, de Vocht F. Static magnetic field effects on human subjects related to magnetic resonance imaging systems. Prog Biophys Mol Biol 2005;87:255–265.
4. Budinger T, Bristol K, Yen C, Wong P. Biological effects of static magnetic fields. New York: ; 1984. p 113–114.
5. Volkow N, Wang G, Fowler J, et al. Resting brain metabolic activity in a 4 Tesla magnetic field. Magn Reson Med 2000;44:701– 705.
6. Cavin I, Glover P, Bowtell R, Gowland P. Thresholds for perceiving metallic taste at high magnetic field. J Magn Reson Imaging 2007;26:1357–1361.
7. Tomasi D, Wang R. Induced magnetic field gradients and forces in the human head in MRI. J Magn Reson Imaging 2007;26:1340–1345.
8. Truong T, Clymer B, Chakeres D, Schmalbrock P. Three-dimensional numerical simulations of susceptibility-induced magnetic field inhomogeneities in the human head. Magn Reson Imaging 2002;20:759–770.
9. Tomasi D, Panepucci H, Vidoto E, Azevedo E. Use of a phase reference for field mapping with amplitude images at low field. J Magn Reson Imaging 1998;131:310–314.
10. Tomasi D, Panepucci, H. Magnetic fields mapping with the phase reference method. Magn Reson Imaging 1999;17:157–160.
11. Haase A, Frahm J, Hanicke W, Merboldt KD. FLASH imaging. Rapid NMR imaging using low flip angle pulses. J Magn Reson 1986;67:257–266.
12. Lee J, Garwood M, Menon R, et al. High contrast and fast three-dimensional magnetic resonance imaging at high fields. Magn Reson Med 1995;34:308–312.
13. Hennig J, Scheffler K. Hyperechoes. Magn Reson Med 2001;46: 6–12.
14. Schenck J. Safety of strong, static magnetic fields. J Magn Reson Imaging 2000;12:2–19.
15. Glover G, Schneider E. Three-point Dixon technique for true water/fat decomposition with B0 inhomogeneity correction. Magn Reson Med 1991;18:371–383.
16. Worsley K, Evans A, Marrett S, Neelin P. A three-dimensional statistical analysis for CBF activation studies in human brain. J Cereb Blood Flow Metab 1992;12:900–918.
17. Schenck J. Physical interactions of static magnetic fields with living tissues. Prog Biophys Mol Biol 2005;87:185–204.
18. Patel M, Williamsom RA, Dorevitch S, Buchanan S. Pilot study investigating the effect of the static magnetic field from a 9.4-T MRI on the vestibular system. J Occup Environ Med 2008;50: 576–583.
19. Wang Z, Chen M, Gong X, Huang W, Xu L, Zhou C. Why cold water delays the onset of vestibular vertigo—a functional MRI study. Eur J Radiol 2008;67:459–465.
20. Schoenfeld M, Neuer G, Tempelmann C, et al. Functional magnetic resonance tomography correlates of taste perception in the human primary taste cortex. Neuroscience 2004;127:347–353.
21. Hu X, Norris DG. Advances in high-field magnetic resonance imaging. Annu Rev Biomed Eng 2004;6:157–184.
22. Kangarlu A, Robitaille P-M. Biological effects and health implications in magnetic resonance imaging. Concepts Magn Reson A 2000;12:321–359.
23. Chakeres D, Kangarlu A, Boudoulas H, Young D. Effect of static magnetic field exposure of up to 8 Tesla on sequential human vital sign measurements. J Magn Reson Imaging 2003;18:346–352.